

**MORPHOLOGICAL PROPERTIES OF ZINC
OXIDE NANOSTRUCTURES PREPARED BY
ELECTROCHEMICAL PROCESS**

MAH CHAI FONG

**UNIVERSITI SAINS MALAYSIA
2018**

**MORPHOLOGICAL PROPERTIES OF ZINC
OXIDE NANOSTRUCTURES PREPARED BY
ELECTROCHEMICAL PROCESS**

by

MAH CHAI FONG

**Thesis submitted in fulfillment of the requirements
for the degree of
Master of Science**

July 2018

ACKNOWLEDGEMENT

First and foremost, I would like to express my gratitude to my supervisor, Dr. Yam Fong Kwong for his guidance and support throughout the project. Without his advice and motivation, it would not be possible for this dissertation to be completed smoothly.

I would also like to thank my research colleagues from the group: Ng Siow Woon, Chai Yingqi, Tan Lay Kim, Chin Ing Khang and Cheong Yuit Ling who willing to share their knowledge to assist me complete my research. With opportunity, I offer my sincerest thanks to Dr. Beh Khi Poay and Dr. Tneh Sau Siong who gave me a hand when I was confused during the project and offered unlimited patience in guiding me for preparing experiments and paper publications.

My appreciation extends to the staff of Nano-Optoelectronic Research and Technology Laboratory (N.O.R Lab) for their technical assistance in operating various equipment during my laboratory work.

Finally, I am most indebted to my parents for their patience, support and care throughout the period I carry out this work. Their selfless love and endless support have pushed me to complete my study on time.

TABLE OF CONTENTS

ACKNOWLEDGEMENT	ii
TABLE OF CONTENTS	iii
LIST OF TABLES.....	viii
LIST OF FIGURES.....	ix
LIST OF ABBREVIATIONS	xiii
LIST OF SYMBOLS	xv
ABSTRAK.....	xvi
ABSTRACT	xviii

CHAPTER 1 - INTRODUCTION

1.1	Nanoscience and nanotechnolgy	1
1.2	Nanomaterials	3
1.3	General view on zinc oxide.....	4
1.4	Research objectives	6
1.5	Novelty.....	6
1.6	Thesis outline	7

CHAPTER 2 - LITERATURE REVIEW

2.1	Introduction	8
2.2	Zinc oxide.....	8

2.2.1	Dimensionality	8
2.2.2	Structural properties and lattice parameters	12
2.2.3	Optical properties and band gap	15
2.3	Fabrication method of ZnO	17
2.3.1	Vapor phase synthesis	17
2.3.1(a)	Molecular beam epitaxy (MBE)	17
2.3.1(b)	Sputtering	18
2.3.1(c)	Chemical vapor deposition (CVD)	19
2.3.2	Solution phase synthesis	21
2.3.2(a)	Sol-gel method	21
2.3.2(b)	Electrochemical method	22
2.4	Application	29
2.4.1	Gas sensor	29
2.4.2	Dye-sensitized solar cell (DSSC)	30
2.5	Summary	32

CHAPTER 3 - MATERIALS AND METHODOLOGY

3.1	Introduction	33
3.2	Method of sample fabrication	33
3.2.1	Electrochemical deposition	34
3.2.1(a)	Chemicals	34
3.2.1(b)	Substrate and electrode	35

3.2.1(c)	Growth of nanostructures (Variation of precursor concentration) ...	36
3.2.1(d)	Post-thermal treatment	36
3.2.2	Anodization	36
3.2.2(a)	Chemicals.....	37
3.2.2(b)	Substrate and electrode	37
3.2.2(c)	Growth of nanostructures (Variation of applied voltage, electrolyte concentration and duration)	38
3.2.2(d)	Post-thermal treatment	39
3.3	Summary of experiment	40
3.4	Characterization tools.....	42
3.4.1	Field emission scanning electron microscopy (FESEM).....	42
3.4.2	Energy dispersive X-ray (EDX) spectroscopy	43
3.4.3	Transmission electron microscopy (TEM)	44
3.4.4	Atomic force microscopy (AFM).....	45
3.4.5	X-ray diffractometer (XRD)	46
3.4.6	Photoluminescence (PL) spectroscopy	49
3.4.7	Fourier transforms infra-red (FTIR) spectrometer	51
3.5	Summary	52

CHAPTER 4 - RESULTS AND DISCUSSION

4.1	Introduction	53
4.2	Electrochemical deposition (Variation of electrolyte concentration)	54

4.2.1	FESEM surface morphological analysis	54
4.2.2	EDX elemental analysis	55
4.2.3	XRD structural analysis	57
4.3	Anodization	59
4.3.1	AFM surface roughness analysis of electrochemical polished substrate ...	59
4.3.2	FESEM surface morphological analysis of as-anodized nanostructures ...	61
4.3.2(a)	Variation of voltage in anodization.....	61
4.3.3(b)	Variation of electrolyte concentration in anodization.....	64
4.3.2(c)	Variation of duration in anodization	66
4.3.3	Growth stages of as-anodized nanostructures	74
4.3.4	Effect of annealing on as-anodized nanostructures.....	79
4.3.4(a)	Morphology analysis (FESEM and TEM).....	80
4.3.4(b)	XRD analysis	81
4.3.4(c)	PL analysis.....	87
4.4	Summary	89

CHAPTER 5 - CONCLUSION AND RECOMMENDATION FOR FUTURE

STUDIES

5.1	Conclusion	91
5.2	Recommendation for future studies	93

REFERENCES 95

APPENDICES

LIST OF PUBLICATION

LIST OF TABLES

		Page
Table 2.1	Comparison between DC and RF sputtering.	18
Table 2.2	List of variants of CVD.	20
Table 2.3	Literature survey on deposition conditions and the resultant ZnO nanostructures.	24
Table 2.4	Literature survey on anodization conditions and the resultant ZnO nanostructures.	27
Table 3.1	Experimental conditions for different electrochemical processes.	34
Table 4.1	The reflectance peaks intensity of as-anodized samples based on FTIR spectrum.	78
Table 4.2	The intensity ratio of the UV and visible peak emission, I_{UV}/I_{VL} based on PL spectra with respect to annealing temperature.	89
Table A.1	FWHM values of XRD diffraction peak (101) and the calculated crystallite size of annealed ZnO nanowires by Scherer equation with respect to annealing temperature.	104
Table B.1	Theoretical, experimental and deviation values of the lattice constant c of annealed ZnO nanowires.	105
Table C.1	Intensity of UV and visible peak emission from PL spectra and its ratio with respect to annealing temperature.	106

LIST OF FIGURES

		Page
Figure 1.1	Applications of nanotechnology.	2
Figure 2.1	SEM image of different types of 0D nanostructures, where (A) quantum dots, (B) nanoparticles arrays, (C) core-shell nanoparticles, (D) hollow cubes and (E) nanospheres.	9
Figure 2.2	SEM image of different types of 1D nanostructures, where (A) nanowires, (B) nanorods, (C) nanotubes, (D) nanobelts, (E) nanoribbons and (F) hierarchical nanostructure.	10
Figure 2.3	SEM image of different types of 2D nanostructures, where (A) nanoplates, (B) nanosheets, (C) nanowalls, (D) nanodiscs and (E) branched-structures.	11
Figure 2.4	SEM image of different types of 3D nanostructures, where (A) nanoballs, (B) nanocoils and (C) nanoflowers.	12
Figure 2.5	Schematic diagram of ZnO crystal structures for (a) rocksalt, (b) zinc blende and (c) wurtzite.	13
Figure 2.6	Atomic arrangement of (a) hexagonal close packed wurtzite ZnO and (b) cross-section structures of wurtzite ZnO.	14
Figure 2.7	PL spectrum of ZnO nanorods grown on Si (001) substrate.	15
Figure 2.8	Energy level responsible for edge emission and visible emission in the band scheme of ZnO.	16
Figure 2.9	Schematic diagram of a ZnO-based DSSC.	31
Figure 3.1	Schematic diagram of electrochemical setup.	33
Figure 3.2	Photo of (a) RF sputtering system and (b) the ITO coated glass slide substrate.	35
Figure 3.3	Photo of polished (left) and unpolished (right) Zn foil.	38

Figure 3.4	Photo of as-anodized Zn foil with white membrane on its surface.	39
Figure 3.5	Flowcharts of the works (a) electrochemical deposition, (b) electrochemical polishing and (c) anodization.	41
Figure 3.6	Schematic diagram of basic components in FESEM system.	42
Figure 3.7	Schematic diagram of basic components in TEM.	44
Figure 3.8	Schematic diagram of AFM.	46
Figure 3.9	Schematic diagram of basic components in XRD.	47
Figure 3.10	Geometry construction of Bragg's Law.	48
Figure 3.11	Schematic diagram of basic components in PL spectrometer.	49
Figure 3.12	Energy diagram showing PL mechanism.	50
Figure 3.13	Schematic diagram of basic components in FTIR system.	51
Figure 4.1	FESEM image of ZnO nanostructures grown on ITO substrate at electrolyte concentrations of (a) 0.05 M, (b) 0.1 M, (c) 0.15 M and (d) 0.2 M.	54
Figure 4.2	EDX spectrum of the ZnO sample that grown with 0.15 M concentration.	56
Figure 4.3	Ratio of [Cl] : [Zn] for the ZnO nanostructures as a function of electrolyte concentration from 0.05 M to 0.2 M.	57
Figure 4.4	XRD patterns of the ZnO sample grown with 0.15 M concentration for as-grown and annealed condition.	58
Figure 4.5	Three-dimensional representations of AFM topographic data for (a) unpolished Zn, (b) electrochemical polished-Zn at 50 mA, (c) 100 mA, (d) 130 mA, (e) 150 mA and (f) 200 mA.	60

Figure 4.6	FESEM images of the (a) nanoplatform formed at 1 V, (b) nanowhiskers grown on nanoplatform at 3 V, (c) ensemble of nanowhiskers into nanoflowers at 5 V and (d) nanoflowers started covering the Zn surface at 10 V.	62
Figure 4.7	Average diameter of nanoflowers against the applied voltage during anodization of 1 min.	63
Figure 4.8	FESEM images of formation of (a) pit at 1 mM, (b) nanoflowers at 10 mM, (c) 30 mM, (d) 50 mM, (e) 70 mM and (f) 100 mM of NaHCO ₃ electrolyte.	64
Figure 4.9	Average diameter of nanoflowers against the electrolyte concentration during anodization of 1 min.	65
Figure 4.10	FESEM surface morphologies of zinc foil (a) after being electrochemical polished, (b) anodizations for 1 s, (c) 4 s, (d) 6 s and (e) 10 s in NaHCO ₃ electrolyte.	67
Figure 4.11	Average diameter of pits against anodization duration.	68
Figure 4.12	FESEM images of the nanostructures grown in pits after anodizations for (a) 2 s, (b) 6 s and (c) 10 s in NaHCO ₃ electrolyte.	69
Figure 4.13	FESEM images of nanoflowers formed after anodizations for (a) 20 s, (b) 50 s and (c) 2 min in NaHCO ₃ electrolyte.	70
Figure 4.14	Average diameter of nanoflowers against anodization duration.	71
Figure 4.15	FESEM images show the transformation of nanoflowers to nanowires after anodization for (a) 3 min (b) become nanowires at 5 min, (c) 15 min and (d) 30 min in NaHCO ₃ electrolyte.	72
Figure 4.16	Average diameter of nanowires against anodization duration.	73
Figure 4.17	Schematic diagram of the evolution of nanowires under various stages during anodization of Zn foil in NaHCO ₃ electrolyte.	74

Figure 4.18	Current-transient profile of Zn anodized in NaHCO ₃ electrolyte at constant 10 V.	76
Figure 4.19	FESEM image of the surface below the nanowires showing a significantly rougher surface that originating from corrosion attack.	77
Figure 4.20	FTIR spectra of the as-anodized sample.	78
Figure 4.21	FESEM images of (a) as-anodized nanowires and (b) annealed nanowires. TEM images of (c) as-anodized nanowires and (d) annealed nanowires.	80
Figure 4.22	XRD patterns of the (a) as-anodized sample and samples that calcinated at different temperature and (b) annealed samples that rescaled from range 30 – 38°.	82
Figure 4.23	Crystallite size of ZnO nanowires against thermal annealing temperature.	84
Figure 4.24	Deviation values of lattice constant <i>c</i> against with annealing temperature.	85
Figure 4.25	PL spectra of as-anodized sample and sample that calcinated at different temperature for 1 hr.	88

LIST OF ABBREVIATIONS

AC	Alternating current
AFM	Atomic force microscopy
ALD	Atomic layer deposition
CVD	Chemical vapor deposition
DC	Direct current
DI	De-ionized
DSSC	Dye-sensitized solar cell
e-beam	Electrons beam
EDX	Energy dispersive X-ray
FESEM	Field emission scanning electron microscopy
FTIR	Fourier transforms infra-red
FWHM	Full width at half maximum
IR	Infra-red
MBE	Molecular beam epitaxy
MOCVD	Metal-organic chemical vapor deposition
PECVD	Plasma-enhanced chemical vapor deposition
pH	Potential of hydrogen
PL	Photoluminescence
RHEED	Reflection high-energy electron diffraction
RF	Radio frequency
TEM	Transmission electron microscopy
UV	Ultra-violet
VLS	Vapor liquid solid

v/v	Volume to volume ratio
XRD	X-ray diffractometer
0D	Zero-dimensional
1D	One-dimensional
2D	Two-dimensional
3D	Three-dimensional

LIST OF SYMBOLS

a	Edge length
c	Height of unit cell
c_o	Lattice constant c value of stress free ZnO
c_{exp}	Lattice constant c value of experimental ZnO
d	Interatomic spacing
D	Crystallite size
k	Dimensionless shape factor
u	Internal parameter
λ	Wavelength
θ	Bragg diffraction angle in degree
β	Full width at half maximum

SIFAT-SIFAT MORFOLOGI NANOSTRUKTUR ZINK OKSIDA SEDIAAN MELALUI PROSES ELEKTROKIMIA

ABSTRAK

Dalam kerja ini, dua kaedah elektrokimia, iaitu deposisi elektrokimia dan anodisasi telah digunakan untuk mensintesis nanostruktur ZnO. Nanostruktur berbentuk kubus telah disintesis dengan kaedah deposisi elektrokimia, di dalam campuran zink klorida (ZnCl_2) dan kalium klorida (KCl) yang sama molar dengan kepekatan yang berbeza telah digunakan sebagai elektrolit. Kesan kepekatan elektrolit terhadap perubahan struktur fizikal pada nanostruktur telah diperhatikan. Saiz purata nanostruktur yang dimendap berkurangan dari 207 nm hingga 102 nm semasa meningkatkan kepekatan elektrolit. Corak difraksi sinar-X (XRD) membuktikan bahawa nanostruktur yang dimendap berubah dari amorf ke heksagonal wurtzite ZnO selepas rawatan haba pada 600°C selama 3 jam. Selain itu, deposisi elektrokimia dalam elektrolit klorida menyebabkan peralihan puncak dalam corak XRD disebabkan penggabungan ion klorida. Anodisasi sebaliknya, telah mensintesis nanowayar dengan anodisasi kerajang zink (Zn) dalam elektrolit natrium bikarbonat (NaHCO_3). Pembentukan nanostruktur yang berbeza telah diperhatikan apabila mengubah parameter tindak balas seperti voltan yang digunakan, kepekatan elektrolit dan tempoh anodisasi. Analisis yang mendalam terhadap fasa-fasa perubahan ini membolehkan peringkat pertumbuhan dicadangkan. Evolusi nanostruktur dengan kaedah anodisasi boleh dikategorikan kepada empat tahap, iaitu berlubang bopeng, pertumbuhan nanostruktur dalam lubang, pembentukan nanobunga dan transformasi kepada nanowayar. Nanowayar yang difabrikasi pada

asalnya bersifat amorf, sementara spektroskopi transformasi fourier infra-merah (FTIR) mendedahkan ikatan kimia dalam nanowayer berkaitan dengan zink hidroksi karbonat atau dinamakan sebagai hidrozinkit. Nanowayer hidrozinkit diubahkan menjadi heksagonal wurtzite ZnO melalui rawatan haba. Keseluruhan bentuk nanowayer dikekalkan selepas rawatan haba tetapi permukaannya telah menjadi berbutir. Ini disebabkan oleh pengecutan diameter nanowayer apabila penyepuhlingkatan yang telah disokong oleh mikroskopi elektron transmisi (TEM). Di samping itu, memanipulasi suhu rawatan haba membantu memperbaiki sifat struktur dan optik nanowayer ZnO. Keamatan yang lebih tinggi daripada puncak pembelauan, lebih sempit pada lebar separuh maksimum (FWHM) serta penurunan dalam nilai deviasi kekisi c dari rujukan standard telah diperolehi dalam analisis XRD. Keputusan ini menunjukkan kualiti kristal ZnO yang lebih baik didapati pada suhu haba yang tinggi. Tambahan pula, nilai I_{UV}/I_{VL} (nisbah intensiti puncak ultraungu kepada puncak pancaran dalam keterlihatan) yang dikira paling tinggi dari spektrum fotoluminesens (PL) ialah 4.09 adalah sangat berhampiran dengan nilai eksperimen terbaik yang dilaporkan dari kesusasteraan.

MORPHOLOGICAL PROPERTIES OF ZINC OXIDE NANOSTRUCTURES PREPARED BY ELECTROCHEMICAL PROCESS

ABSTRACT

In this work, two electrochemical methods, i.e. electrochemical deposition and anodization have been used to grow ZnO nanostructures. Cube-like nanostructures has been synthesized by electrochemical deposition, in which a mixture of equimolar zinc chloride (ZnCl_2) and potassium chloride (KCl) with different concentration has been served as electrolyte. The effect of electrolyte concentration against the physical structural changes on the nanostructure was observed. The average size of the deposited nanomaterial was decreased from 207 nm to 102 nm with increase of electrolyte concentration. X-ray diffraction (XRD) pattern revealed the as-deposited nanostructures were converted from amorphous to hexagonal wurtzite ZnO phase after heat treatment at 600 °C for 3 hours. Besides that, electrochemical deposition in chloride medium has caused peak shift in XRD patterns due to the incorporation of chloride ions. Anodization on the other hand, has synthesized nanowires by one-step anodizing zinc (Zn) foil in basic sodium bicarbonate (NaHCO_3) solution. The formation of different nanostructures was observed when varying the reaction parameters such as applied voltage, electrolyte concentration and anodizing duration. An in-depth analysis of these changing phases enabled a growth stage to be proposed. The evolution of as-anodized nanostructures can be categorized into four stages, i.e. pitting, growth of nanostructures in pit, formation of nanoflowers and transformation to nanowires. The fabricated nanowires originally was amorphous in nature, whilst the fourier transform infra-red

spectroscopy (FTIR) measurement revealed the chemical bonds within the nanowires attributed to zinc hydroxy carbonate or commonly named as hydrozincite. Hydrozincite nanowires were converted into hexagonal wurtzite ZnO through heat treatment. The overall nanowires form was preserved after annealing yet its surface became granular. This is due to contraction in diameter of nanowires upon annealing as supported by evidence from transmission electron microscopy (TEM). In addition, manipulating the annealing temperature has improved the structural and optical properties of ZnO nanowires. Higher intensities of diffraction peaks, narrower in full width at half maximum (FWHM) as well as the decrease of deviation values of lattice constant c from the standard reference was obtained in XRD analysis. These results implied better crystalline quality of ZnO has been fabricated at high annealing temperature. Furthermore, the highest calculated value of I_{UV}/I_{VL} (the intensity ratio of the ultraviolet to the visible peak emission) from photoluminescence (PL) spectrum was found to be 4.09 which is close to the best experimental value reported from literature.

CHAPTER 1

INTRODUCTION

1.1 Nanoscience and nanotechnology

Nanoscience and nanotechnology involve studying and working with matter on an ultra-small scale through various scientific areas, such as chemistry, biology, physics, materials science, and engineering. This idea was first introduced by Richard Feynman in the talk entitled “There’s Plenty of Room at the Bottom” in 1959 (Feynman, 1960). He described a technological vision of extreme miniaturization and challenged scientists to explore this new scientific field. However, his talk did not inspire conceptual beginnings of the field during that time. Until in the year 1974, his concept was rediscovered and publicized in a conference paper by Professor Norio Taniguchi. Since then, this field has gathered considerable attention and started to develop. It has been estimated that total investment in nanotechnologies from governments and industries around the world was around 5 billion euros in the past decades (Society and Engineering, 2004). Aside from that, the numbers of published patents in nanotechnology have increased fourfold within 6 years (ISI Web of Knowledge).

Nanotechnology has a profound impact on many aspects of our lives. The examples of its participated areas are shown in Figure 1.1.

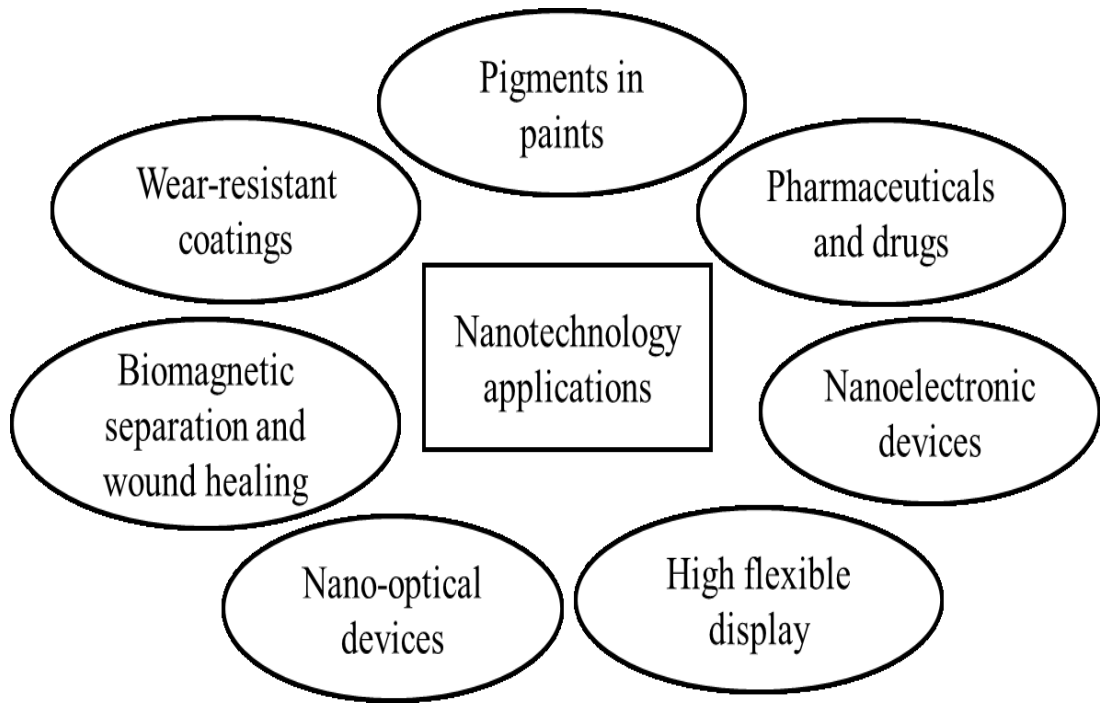


Figure 1.1: Applications of nanotechnology (Council, 2002).

The application of nanotechnology is started to grow rapidly at early 2000's and it was found to be used in producing nanoscale materials in their free form without consolidation or blending (Council, 2002). The product, nanomaterials were then widely used in our daily goods. For example, nanoscale zinc oxide (ZnO) and iron oxide (Fe_2O_3) powder are used in cosmetics manufactures for sunscreen lotions and lipstick (Lu et al., 2015). Paints with reflective properties are also being manufactured using nanoscale titanium dioxide (TiO_2) powder (Markowska-Szczupak et al., 2011). Aside from that, nanostructured wear-resistant coatings are used on cutting tools and Navy ships to increase their durability (Ireni et al., 2017; Markowska-Szczupak et al., 2011).

After that, more sophisticated uses of nanoscale materials have been realized and it started to involve in the areas of information technology and medical development. In the information technology area, smaller and more power-efficient

components have been manufactured and substantially increase the information storage density such as hard disk drives that are manufactured in micro-size but are able to have storage up to several terabytes. Besides that, development in nanocrystalline has driven larger area, higher brightness and flat-plane displays for television screens and computer monitors. While, in medical areas, nanoscale matters such as magnetic nanoparticles, fluorescent nanospheres and liposome have promoted to speed up separation and selection of blood/other body fluids, wound detection, improve delivery of therapeutic agents and etc (Jebali et al., 2017; Mohammed et al., 2017).

Since nanoscale technologies span a much broader range of scientific applications than those microscale technologies, it will certainly continue to grow in various areas and many new properties and applications will be discovered.

1.2 Nanomaterials

The formation of nanomaterials can be categorized as ‘top-down’ and ‘bottom-up’ methods (Society and Engineering, 2004; Council, 2002). Producing very small structures from large pieces of materials is ‘top-down’ technique, while, growing from atom by atom or molecule by molecule (self-assembly) is ‘bottom-up’ technique. The examples for these two methods are etching to create circuits on the surface of silicon (Si) microchip and crystals grown for the semiconductor materials, respectively.

Nanomaterials are things that manufactured at a very small scale (less than 100 nm in size) and they are widely developed to exhibit novel characteristics compared to the same material without nanoscale features. The properties of materials at nanoscale are different for two main reasons. First, nanomaterials have a

relatively larger surface area to volume ratio when compared to the same mass of material produced in a larger form. This can enhance the materials characteristics such as reactivity, strength and electrical properties (Eriksson et al., 2009; Roduner, 2006). As the particle in bulk material decreases in size, the active surface areas are greatly increased and thus have faster reaction.

Second, the particles in nanomaterials are small enough to confine the electron motion and quantum effects could be induced. Quantum effect can change the properties of a nanomaterial such as melting point, optical properties, magnetic properties and etc (Filipponi et al., 2010; Roduner, 2006; Society and Engineering, 2004). For example, gold nanoparticles melt at much lower temperatures (~ 300 °C) than the gold slabs (1064 °C). Moreover, gold and silver appear in unexpected color against its particles size. In size of 10 – 40 nm, gold particles exhibit a red color and silver particles exhibit a blue color. While, in size of ~ 100 nm, they appear purple and yellow, respectively. On the other hand, quantum confinement will give rise to a magnetoresistance effect in magnetic materials. This property is being used in data storage and sensing devices by a combination of multilayers of strong ferromagnetic and non-magnetic buffer.

In other words, the properties of nanomaterials can be size-dependent as they no longer follow Newtonian physics but rather quantum mechanics. This unique characteristic makes them an exceptional class of materials to be studied.

1.3 General view on zinc oxide

Zinc oxide is an inorganic compound with the empirical formula ZnO. It can be produced by two different methods: indirect process and direct process (Porter, 1991). Indirect process is also known as the France process as it was popularized by

a French name LeClaire in 1844. In the indirect process, metallic zinc is firstly melted and vaporized at temperature above 1000 °C, and then the zinc vapor is reacted with the oxygen in atmosphere to form ZnO. While, the direct process starts with diverse contaminated zinc composites such as zinc ores. This zinc source is heating with a source of carbon to produce zinc vapor (carbothermal reduction), which is then oxidized as in the indirect process. Because of low purity of the source material, the final product ZnO is also of lower quality as compared to the indirect process.

At room temperature, ZnO powder is white in color, but upon heating, it changes to yellow. This visual change is an important hint for researchers to speculate the fabricated sample may be zinc (Zn) related compound and can be converted to ZnO through annealing. The color change is caused by small loss of oxygen to the environment at high temperatures to form the non-stoichiometric $Zn_{1+x}O$ (Wiberg et al., 2001).

ZnO is a II-IV group semiconductor with broad energy band (3.3 eV) and high binding energy (60 meV) which enables it to sustain large electric fields and permits excitonic emission at room temperature. Due to these properties, ZnO has been extensively used in optoelectronic devices fabrication such as light emitting diodes, solar cell, ultra-violet (UV) photodetector and gas sensor (Özgür et al., 2010; Zhang et al., 2012). Apart from that, ZnO is also used as an additive in industrial products. It is added into rubbers, ceramics, paints, sunscreen, and lubricants to enhance their properties (Hernández Battez et al., 2008).

With its vast applications, study on ZnO material has shown an increment. As much as 100 thousand related papers on fabrication of ZnO can be found from the internet and has an average increment of 15% in each year (ISI Web of Knowledge).

1.4 Research objectives

The objectives of this project are:

1. To study and characterize the ZnO nanomaterials grown by two different electrochemical processes, i.e. electrochemical deposition and anodization.
2. To examine the formation of anodized-Zn nanostructures and propose a suitable growth stage.
3. To study the effects of annealing temperature on the properties of anodized-Zn nanostructures.

1.5 Novelty

This project investigates different fabrication parameters of ZnO nanostructures through cost efficient electrochemical methods. Cube-like ZnO nanostructures are synthesized by electrochemical deposition under low temperature. On the other hand, one-dimensional (1D) ZnO nanostructures are successfully fabricated by one-step anodization in chemically mild conditions. From literature, anodization of Zn is scarcely studied as compared with other metals due to Zn being a reactive metal and its oxide form is easily dissolved in acidic or alkaline electrolytes that are commonly used during experiment. Moreover, growth of 1D ZnO nanostructures in one step typically requires high temperature, a limited choice of substrates and a costly setup.

In addition, chronological growth stages of anodized-Zn nanostructures are studied. The evaluation of the anodized-Zn nanostructures during anodization is presented and so it provides a better understanding in precise control/modification on future studies. Besides that, it is interesting to note that, after annealing, the

fabricated sample has experienced internal changes but the overall shape has been preserved.

1.6 Thesis outline

Other than the brief introduction, research objectives and novelty of this project that have been addressed in chapter 1, this thesis contains several other chapters.

Chapter 2 encompasses more detailed literature review on ZnO, including the type of nanostructures, fundamental properties, fabrication techniques and potential applications.

Chapter 3 provides experimental details on the materials used in this project and the fabrication steps in preparing the samples. In addition, the theory of characterization equipment that involved in this project is also covered.

Chapter 4 presents the characterization results of the synthesized ZnO nanostructures. Subsequently, analysis and discussion on those results are addressed.

Chapter 5 summarizes the major finding in current work and future work is suggested.

CHAPTER 2

LITERATURE REVIEW

2.1 Introduction

This chapter reviews the characteristics of ZnO nanostructures. Aside from that, in addition to the electrochemical methods which are employed in this project, other fabrication approaches are examined. Lastly, we review the potential applications of ZnO nanostructures.

2.2 Zinc oxide

2.2.1 Dimensionality

From literatures, hundreds of novel ZnO nanostructures have been synthesized and they can be mainly classified into four types: zero-, one-, two-, and three- dimensional structures. Zero-dimensional (0D) ZnO nanostructures are usually exhibited in uniform particles sphere shape such as quantum dots, nanoparticles arrays, core-shell nanoparticles, hollow cubes and hollow sphere, as shown in Figure 2.1.

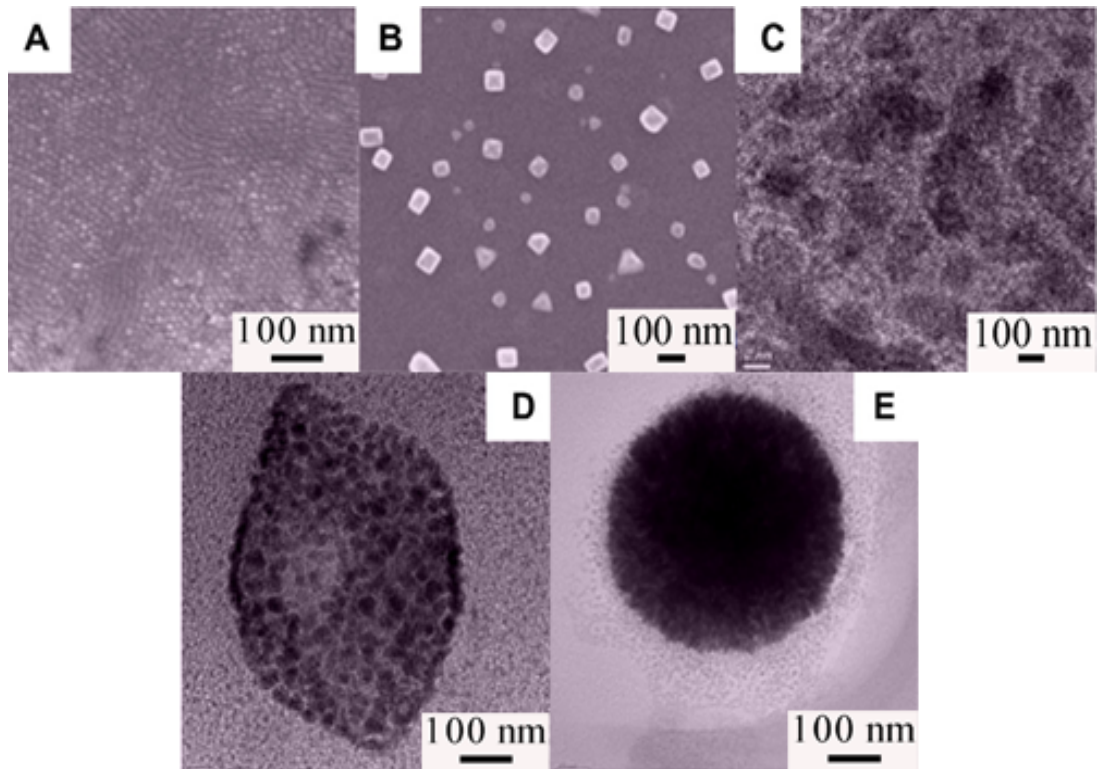


Figure 2.1: SEM images of different types of 0D nanostructures, where (A) quantum dots, (B) nanoparticles arrays, (C) core-shell nanoparticles, (D) hollow cubes and (E) nanospheres (Tiwari et al., 2012).

Literally, 0D nanostructures have the smallest nanoscale size among the group. Its sufficient small dimension could induce quantum effect and this property should have gathered great interest in devices application. Yet, there are difficulties in determining the structures and properties of 0D nanostructures (Demiroglu, 2014). Thus, application of 0D nanostructures in devices manufacturing is relatively new as compared with other dimensional nanostructures.

On the other hand, types of 1D nanostructures make the largest group which includes nanobelts, nanorods, nanoneedles, nanowires, nanorings, nanoribbons and nanocombs (Demiroglu, 2014; Tiwari et al., 2012). Figure 2.2 shows the examples of 1D ZnO nanostructures that have been synthesized in most laboratories.

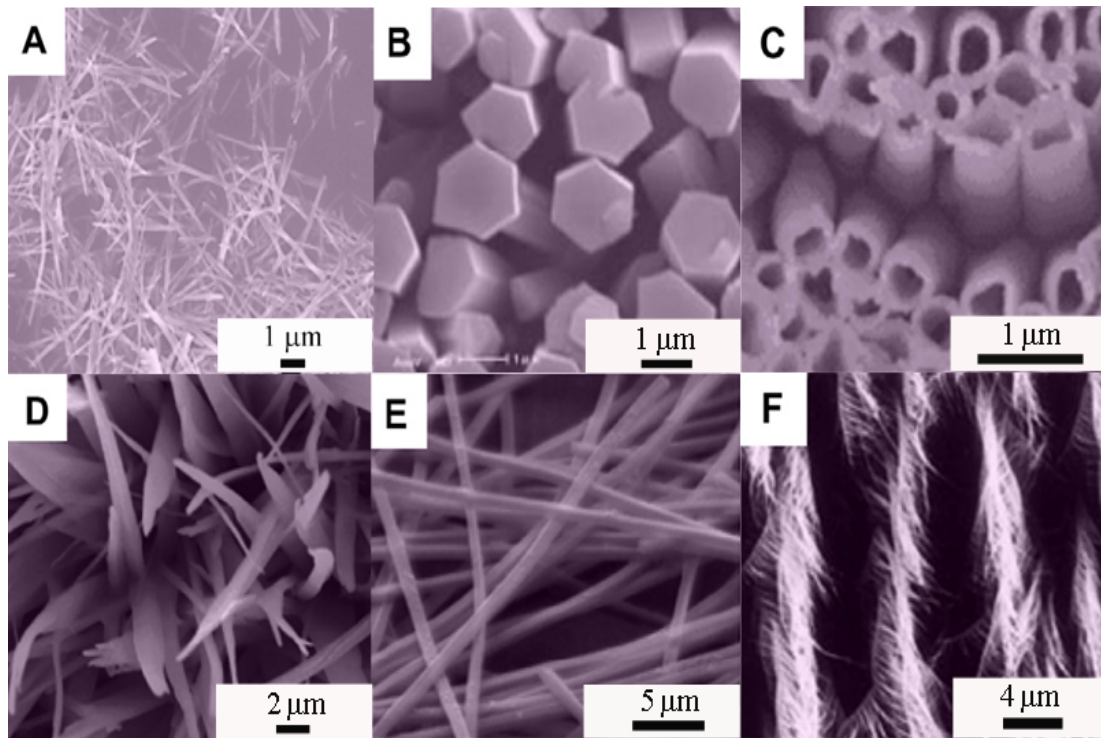


Figure 2.2: SEM images of different types of 1D nanostructures, where (A) nanowires, (B) nanorods, (C) nanotubes, (D) nanobelts, (E) nanoribbons and (F) hierarchical nanostructure (Tiwari et al., 2012).

1D nanostructures have a profound impact in device applications as they provide larger active surface area to volume ratio and can be easily modified to give hierarchical structures which could appreciably increase device efficiency. Pan et al. reported that the response and recovery time of nanocombs ZnO in nitrogen (N_2) gas sensor is 28-fold faster compared to nanowires (Pan et al., 2015).

Two-dimensional (2D) nanostructures have two dimensions outside of the nanometric size range, thus they exhibited in plate-like shape. They include nanoplates, nanosheets, nanowalls, nanodiscs and branched-structures, as shown in Figure 2.3.

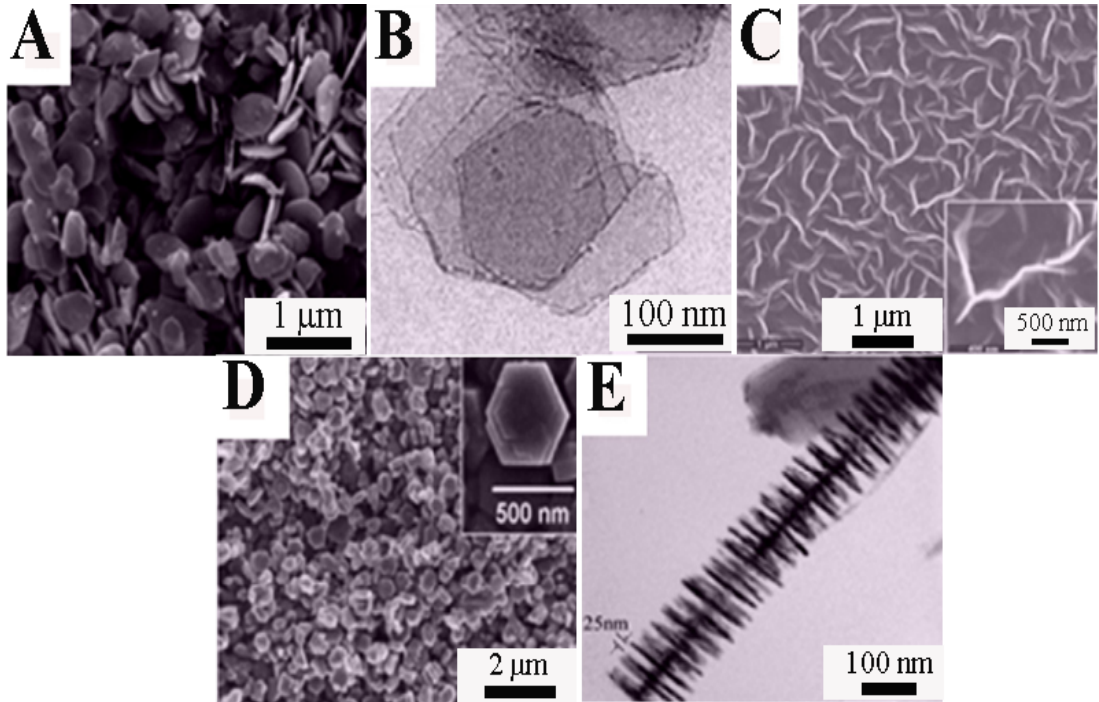


Figure 2.3: SEM images of different types of 2D nanostructures, where (A) nanoplates, (B) nanosheets, (C) nanowalls, (D) nanodiscs and (E) branched-structures (Tiwari et al., 2012).

2D nanostructures are common product that can be observed during fabrication, owing to the stability growth of 2D surface structures (Demiroglu, 2014). For example, Ramirez Canon et al. reported, 2D arrays ZnO are predominant products in anodization of Zn foil process regardless of the potential of hydrogen (pH) of electrolyte (Ramirez Canon et al., 2013). In the report, different types of acid and alkaline electrolytes were used to synthesize ZnO nanostructures, yet, only 2D ZnO are obtained.

Three-dimensional (3D) nanostructures also described as bulk-structures with packing of atom and agglomerate/extend to nearly macroscopic scale. Figure 2.4 shows the 3D ZnO nanostructures such as nanoballs, nanocoils and nanoflowers.

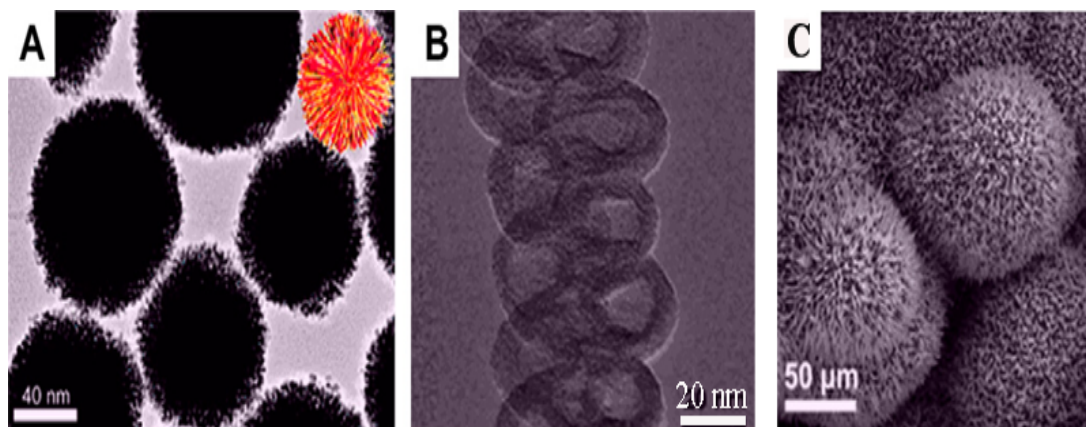


Figure 2.4: SEM images of different types of 3D nanostructures, where (A) nanoballs, (B) nanocoils and (C) nanoflowers (Tiwari et al., 2012).

Lately, 3D ZnO have attracted research interest because this large surface area nanostructure could have porosity in three dimensions that would lead to better transport of molecules and supply enough absorption sites during reaction. Shen et al. reported, these dimensional nanostructures exhibit good activity for oxidation and detection, making them potentially useful in electrocatalytic applications (Shen et al., 2008).

2.2.2 Structural properties and lattice parameters

Three crystalline structures could be found in ZnO, namely hexagonal wurtzite, zinc blende, and rocksalt (Hanada, 2009; Özgür et al., 2005). These crystal structures are constituted of distorted tetrahedral ZnO in different manners as depicted in Figure 2.5.

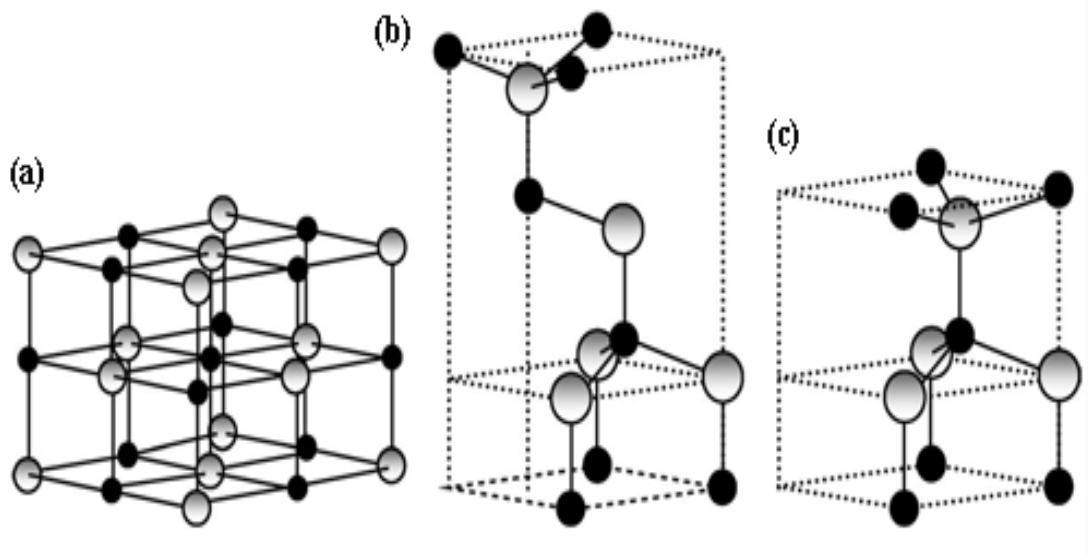


Figure 2.5: Schematic diagram of ZnO crystal structures for (a) rocksalt, (b) zinc blende and (c) wurtzite (Özgür et al., 2005). *Note:* Shaded gray and black sphere represent Zn and O atoms, respectively.

Nevertheless, only wurtzite structures will be given attention in this project.

Wurtzite ZnO is commonly seen in most of the literature because it is thermodynamically stable under ambient conditions (Hanada, 2009; Özgür et al., 2005). Figure 2.6 (a) shows the hexagonal close packed lattices structure of wurtzite ZnO, every atom of one kind (group II atom) is surrounded by four atoms of the other kind (group VI atom) or vice versa, which are coordinated at the edges of a tetrahedron.

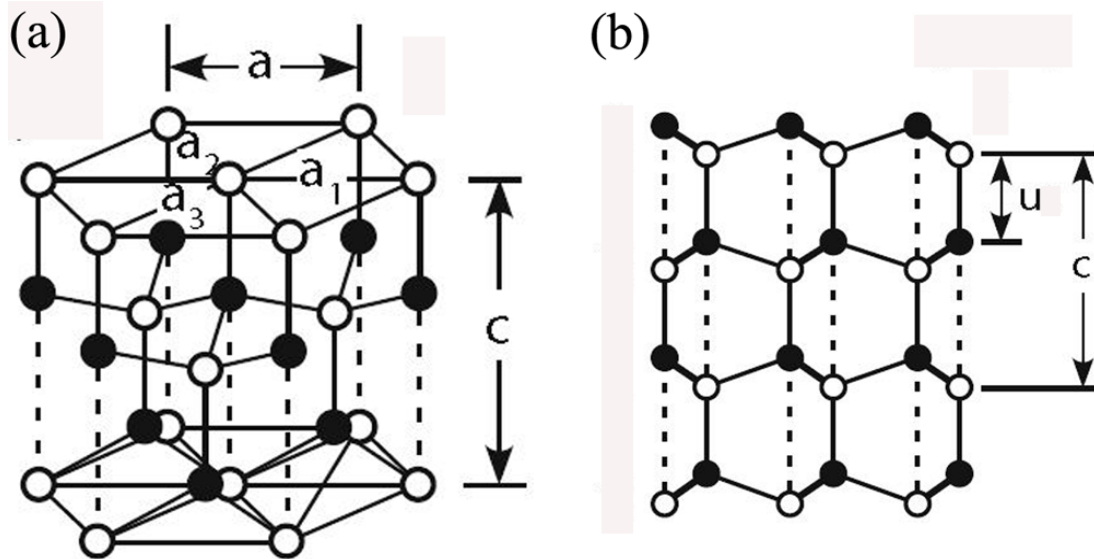


Figure 2.6: Atomic arrangement of (a) hexagonal close packed wurtzite ZnO and (b) cross-section structures of wurtzite ZnO (Hanada, 2009). *Note:* Black circle, white circle, thick solid line and dashed lines represent cation, anion, bonding between two atoms and electrostatic attraction of two atoms, respectively. The symbols ‘ a ’, ‘ a_1 ’, ‘ a_2 ’, ‘ a_3 ’, ‘ c ’ and ‘ u ’ are edge lengths of the unit cell, distance between two atoms, high of the unit cell and internal distance, respectively.

The wurtzite structure composed of arranged alternating biatomic planes, thus, the stacking sequence is $AaBbAaBb\dots$ meaning a mirror image structure. Meanwhile, the distance between this repeated sublattice is known as u , the internal parameter.

In an ideal wurtzite crystal, lattice constants a (edge length) and c (height of unit cell) have relation as $c/a = 1.633$ and internal parameter $u = 3/8 = 0.375$ (Hanada, 2009; Özgür et al., 2005). However, there are pairs of cation and anion atoms connected by dashed lines that attracted to each other by electrostatic force, as shown in Figure 2.6 (b). The iconicity of these bonds is large due to its II–VI group compound, therefore, the length of the dashed lines tends to be shorter than the ideal one. As a result, the experimental c/a ratio is smaller than ideal and u value larger than ideal. This deviation occurs such that the four tetrahedral distances are kept roughly constant in lattice. Experimentally, the values of u and c/a for wurtzite ZnO

were determined in the range where $u = 0.383 - 0.3856$ and $c/a = 1.601 - 1.6035$, as $c = 5.2042 - 5.2075 \text{ \AA}$ and $a = 3.2475 - 3.2501 \text{ \AA}$ (Özgür et al., 2005).

2.2.3 Optical properties and band gap

Typically, ZnO crystal exhibits two emission bands: UV emission band and visible emission band which can be examined by photoluminescence (PL) measurement. Figure 2.7 shows the PL spectrum from ZnO that consists of UV emission band and a broad visible emission band.

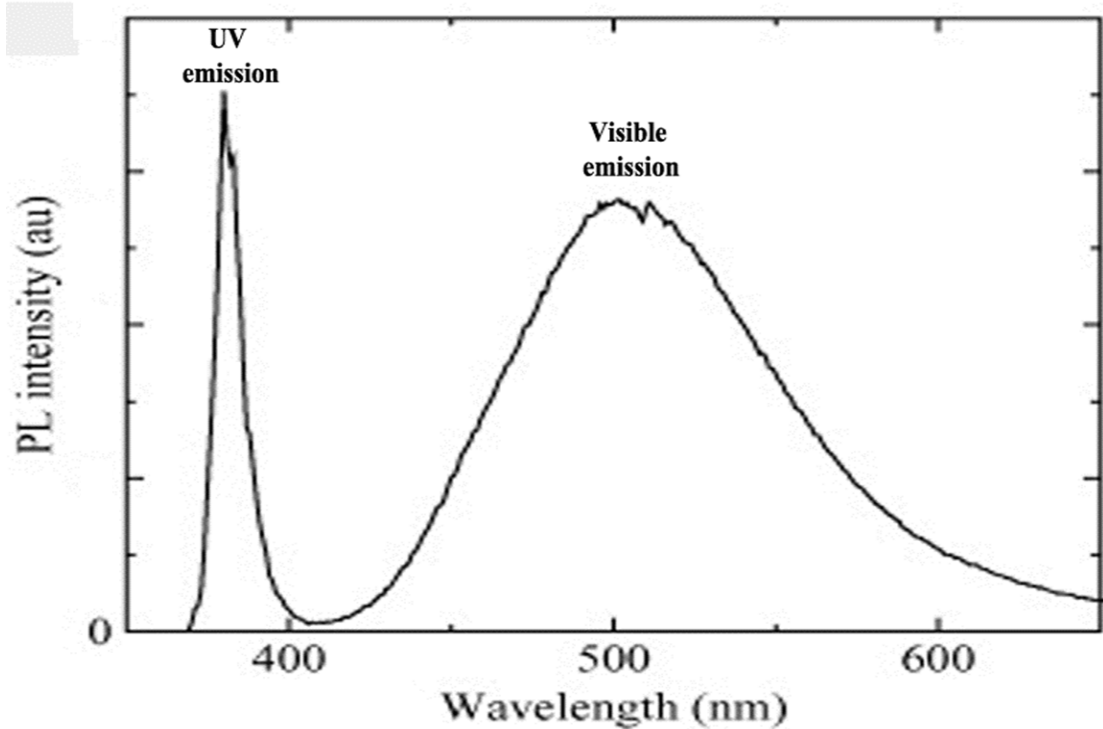


Figure 2.7: PL spectrum of ZnO nanorods grown on Si (001) substrate (Yang, 2008).

To understand the mechanism behind UV and visible emission, let us consider a basic model of electronic transition between different levels of position, as shown in Figure 2.8.

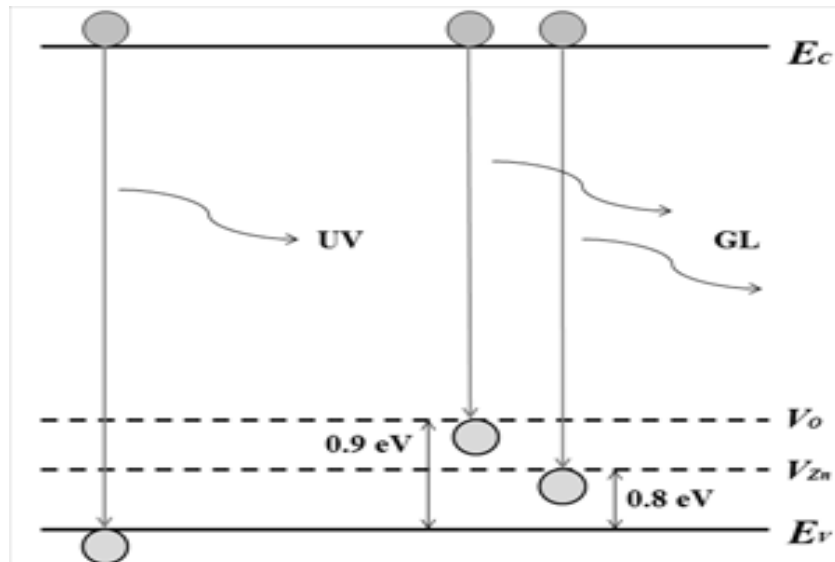


Figure 2.8: Energy level responsible for edge emission and visible emission in the band scheme of ZnO (Rodnyi and Khodyuk, 2011). *Note:* E_c , V_o , V_{zn} , E_v , UV and GL represent conduction band, oxygen vacancy band, Zn vacancy band, valence band, ultra-violet and green luminescence, respectively.

The UV emission band is related to a near band-edge transition or namely the recombination of free excitons (Rodnyi and Khodyuk, 2011; Yang, 2008). Band edge here refers to the highest energy state that an electron can exist at its valence band, and the lowest energy an electron can have in the conduction band. When one electron has energy equal to or near the band gap energy, it would be excited from valence band to conduction band and de-excited back to its steady state, valence band. As it falls, a photon of the exact same energy with the band gap is released. The band gap energy of ZnO is 3.37 eV, the emission is UV luminescence with wavelength of 380 nm.

The broad visible emission band is also known as green emission band, usually centered around 500 nm. Green luminescence is caused by the electronic transitions between shallow donors and deep acceptors that related to intrinsic defects such as oxygen vacancy, Zn vacancy, oxygen interstitial and Zn interstitial (Yang, 2008; Güell et al., 2016; Laurent et al., 2008). Defects in ZnO arise at

different level positions across the band gap, for example, ground level of Zn vacancy lays 0.8 eV higher than the valence band edge and ground level of oxygen vacancy is 0.9 eV above the valence band (Rodnyi and Khodyuk, 2011). The recombination of electron of conduction band with the holes at ground levels would emit photon with longer wavelength due to decrease in energy band gap, thus green luminescence is obtained.

2.3 Fabrication method of ZnO

Several methods have been developed to synthesize ZnO and they can be classified into two groups: vapor phase synthesis and solution phase.

2.3.1 Vapor phase synthesis

2.3.1(a) Molecular beam epitaxy (MBE)

MBE is one of the typical vapor phase synthesis for epitaxial growth of nanostructures on a substrate in an ultra-high vacuum conditions via interaction of one or several molecular or atomic beams. The term epitaxy means surface arrangement, refers to deposition of a monocrystalline thin film onto monocrystalline substrates. MBE was firstly developed by Cho and Arthur in early 1970s to grow GaAs and then evolved into grow of other classes of materials such as III-V compound, IV-VI compound and metal oxide in the following decades (Franchi, 2013).

MBE has achieved numerous successes in synthesizing excellent uniform and low defect concentration ZnO thin films, for example, the full width at half maximum (FWHM) value of ZnO (002) peak as small as 0.04 °, strong narrow band

edge of free exciton emission was obtained in low-temperature PL spectrum and streaky reflection high-energy electron diffraction (RHEED) pattern could be observed (Ko et al., 2000; Kumar et al., 2015; Opel et al., 2014). Besides that, with the assist of advance MBE system such as laser-MBE or plasma-assisted MBE, ZnO can be easily doped with ternary alloy and complex layer-by-layer growth of heterostructures can be well controlled (Kumar et al., 2015; Triboulet, 2001). In short, MBE plays an important role in precise and high quality composition growth.

2.3.1(b) Sputtering

Sputtering technique is another vapor phase synthesis that commonly used to fabricate ZnO thin film. Depending upon the nature of the target, different types of sputtering methods would be used (Schuler, 2008). Table 2.1 summarizes the properties and differences between these two methods: direct current (DC) sputtering and radio frequency (RF) sputtering.

Table 2.1: Comparison between DC and RF sputtering.

DC sputtering	RF sputtering
• Using Zn target	• Using ZnO target
• Sputtering gas Ar	• Sputtering gas Ar
• Reactive gas O ₂	-
• DC power	• AC power

DC sputtering involved the ignition of plasma through a DC bias between a cathode (target) and an anode (substrate) in a vacuum chamber. High purity argon (Ar) and oxygen (O₂) gas are pumped into the chamber for the oxidation of the metallic Zn

target. When the gaseous molecules are ionized, they will be accelerated and bombard the target material causing atoms to be “sputtered” off. These vaporized atoms are then deposited as a thin film on the substrate when they condensed. On the other hand, RF sputtering involves in alternating the electrical potential of the current in the vacuum chamber at radio frequencies. In the first cycle, the non-metallic ZnO target is given negative charge and the ionized sputtering gas atoms are attracted to the target where then polarized the surface ZnO atoms. During the second cycle, when target is given positive charge, the sputtering gas ions together with ZnO atoms are ejected due to reverse polarization and atoms are accelerated toward substrate where deposition takes place.

As the deposition flows are different, the fabricated ZnO thin films have carried different characteristics. DC sputtering produced ZnO with larger grain size of approximately 200 nm (Schuler, 2008). Bigger grain size promotes the formation of highly resistive grain boundaries that inhibit charge transfer between individual grains which is suitable to analyze the piezoelectric properties of a sample (Schuler et al., 2005). While, RF sputtered ZnO has average grain diameter about 50 nm and surface roughness of 7 nm (Schuler, 2008). Smaller grain sizes allow efficient transport of both electron and optical excitation that improved devices’ performance (Ghosh et al., 2014).

2.3.1(c) Chemical vapor deposition (CVD)

CVD technique is widely involved in materials processing technology to produce high-purity bulk materials/powders and solid thin-film coatings to surfaces. The CVD process begins with flowing of precursor gas or gaseous into a chamber containing heated substrates to be coated. A series of chemical reactions, gaseous

reductions and diffusion of precursors would then occur in both the gas phase and on the substrate surface to deposit nanostructures. This is accomplished by the by-products which they are exhausted out of from the chamber along with unreacted precursor gaseous.

CVD have been used to deposit a very wide range of materials at about 70% of the elements in the periodic table, some in the form of pure element, but more often combined to form compounds (Creighton and Ho, 2001). As would be expected with the large variety of materials deposited, there are many derivatives of the CVD terminology such as metal-organic chemical vapor deposition (MOCVD), plasma-assisted or plasma-enhanced chemical vapor deposition (PECVD), atomic layer deposition (ALD) and vapor liquid solid (VLS) growth. Their explanations and respective fabricated nanostructures are summarized in Table 2.2.

Table 2.2: List of variants of CVD.

Method	Properties	Structures	Ref.
MOCVD	<ul style="list-style-type: none"> Utilizes metal-organic precursors 	Thin films	1, 2
PECVD	<ul style="list-style-type: none"> Electrical energy is used to initiate reactions Low growth temperature 	Thin films	1, 3
ALD	<ul style="list-style-type: none"> Gaseous precursors are introduced alternately Superior step-coverage of lattice 	Bulk-like nanostructures	1, 4
VLS	<ul style="list-style-type: none"> Liquid metal droplets as catalysts 	Nanostructures	5, 6

1. (Jones and Hitchman, 2009)
2. (Muthukumar et al., 2003)
3. (Li et al., 2002)
4. (Iqbal et al., 2016)
5. (Zhao et al., 2007)
6. (Zhang et al., 2012)

2.3.2 Solution phase synthesis

2.3.2(a) Sol-gel method

Literally, “sol-gel” refers to the transformation of material from liquid-form sol to solid-form gel. The “sol” refers to dispersion of colloidal particles that has a liquid phase whereas “gel” is colloid in more solid form to a sol (Hench and West, 1990). A colloidal gel consists of combinations of diversity substances that have continuous chain structure to agglomerate the colloidal particles. Therefore, sol-gel method is to dissolve one or more compounds in a solvent and later reform into solid form.

The first step of sol-gel process begins with mixing of colloidal particles in water/alcohol at a pH that prevents precipitation as the sol. With time, the colloidal particles are link together to become a bridged-network (the gel) through polycondensation or polyesterification reaction. Then, the gel is left for period of time, hours to days for aging purpose. During aging, polycondensation and reprecipitation reactions continue along with localized solution which increases the thickness of the gel network and decreases the porosity of the gel. After complete condensation, the gel goes through drying and dehydration process to remove the volatile liquids/water and surface-bound (M-OH) groups from the gel to form a chemically stable solid gel. Lastly, heating the gel at high temperatures is needed to cause densification and decomposition. This method is widely used to prepare various forms of ZnO not limited to thin film but includes also powders, porous structures and fibers (Cushing et al., 2004; Dutta and Basak, 2008; Hench and West, 1990).

2.3.2(b) Electrochemical method

An electrochemical process is a chemical reaction that either causes or is caused by the movement of electrical current between electrodes and electrolyte. This reaction is named as redox reaction. The term ‘redox’ stands for reduction-oxidation where oxidation and reduction describe the change of oxidation state that takes place in the atoms, ions or molecules (Cifarelli et al., 2013; Zawodzinski et al., 2006). Oxidation state is an indicator for the degree of loss of electron which can be positive, negative or zero. For example, an atom that gives up an electron to another atom/ion has its oxidation state increased (positive value), and the recipient of the negatively charged electron has its oxidation state decreased (negative value).

Formally, the set up for electrochemical process is called a electrochemical cell. This kind of cell includes galvanic cell or voltaic cell dependent on it is with voltage or current supply. Typical electrochemical cells have two conductive electrodes, the anode and cathode. The anode is defined as the electrode where oxidation occurs whereas the cathode is the electrode where the reduction takes place (Cifarelli et al., 2013; Zawodzinski et al., 2006). Therefore, if substrate is placed at anode, the electrochemical process known as anodization whereas if substrate placed in cathode known as electrodeposition.

Electrochemical deposition process of materials is reduction of ions from electrolyte, as presented in Equation (2.1) (Paunovic and Schlesinger, 2006).



There are three fundamental steps are involved in the process presented by the equation (2.1). (1) Metal–solution interface as the locus of the deposition process: it consists of two simultaneous reactions, separation of ions from the lattice and interaction of the ions with electrolyte molecules. By supplying current externally,

the ion-ion bond in lattice is broken down and the ions are dissolved in electrolyte then interact with electrolyte molecules. (2) Kinetics and mechanism of the deposition process: the free moving ions in the electrolyte transfer from anode and diffuse to cathode (substrate) so that chemical reaction can take place. (3) Nucleation and growth of the material: the arrival and adsorbed ions then form lattices on the substrate surface and become crystalline material with increasing of time.

Electrodeposition with different operating parameters is likely to produce different kinds of deposit structures. Table 2.3 summarizes some of the examples on the effects of operating parameters towards the morphology growth of ZnO.

Table 2.3: Literature survey on deposition conditions and the resultant ZnO nanostructures.

Deposition condition variable	FESEM	XRD	Ref.
Different Metal Oxide Underlays: a) ITO/glass substrates b) FTO/glass substrates c) ZnO seed layers on ITO/glass substrates d) ZnS substrates e) TiO ₂ substrates	Nanorods a) diameter, d~170 nm b) diameter, d~300 nm c) diameter, d~200 nm d) diameter, d~150 nm e) diameter, d~60 nm	Preferably growth along (002) plane	1
Different concentration of electrolyte: (Zn(NO ₃) ₂ •6H ₂ O + Zn(NO ₃) ₂) a) 0.005 M b) 0.01 M c) 0.02 M d) 0.03 M	Inclination (the angle between the normal to the thin film surface and the nanorods) of ZnO nanorods increased	Intensity of diffraction peak (002) increased	2
Different deposition temperature: a) 60 °C b) 70 °C c) 80 °C d) 90 °C	Size of the ZnO grain decreased	Diffraction peaks shifted to smaller angles	3
Different deposition time: a) 10 min b) 20 min c) 40 min d) 60 min	Density of nanorods increased	Intensity of diffraction peak (002) increased	4